PDF Modeling of Turbulent-Mixing Effects on Initiator Efficiency in a Tubular LDPE Reactor

Kuochen Tsai and Rodney O. Fox
College of Engineering, Kansas State University, Manhattan, KS 66506

The effect of turbulent mixing in the reaction zone of a tubular low-density polyethylene reactor was studied by combining a Lagrangian composition probability density function (LCPDF) code with a computational fluid-dynamics code. Because the LCPDF code can treat the chemical reaction terms in a turbulent flow without resorting to moment closures, it is used to describe the temperature and scalar fields of reactants including initiator and monomer molar concentrations, and the moments of the molecular weight distribution. The chemical reaction terms are efficiently dealt with using a three-parameter chemical lookup table that contains the temperature and composition changes as functions of initiator and monomer concentrations and temperature over a small time step. The reaction-rate constants from the study of Lee and Marano (1979) are functions of temperature and pressure. The flow fields are obtained using the $k-\epsilon$ turbulence model. Because the temporal and spatial evolution of all fields in the reactor can be simulated, it is possible to study the effect of the initiator injection location, flow rate and temperature of the monomer and initiator feed streams on polymerization in considerable detail. Moreover, by observing the probability distribution of the composition fields, a better understanding of hot-spot formation is achieved, leading to improved reactor designs.

Introduction

Low-density polyethylene (LDPE) polymerization in plant-scale reactors has long been an important research topic in industry due to commercial competition and the difficulties in reactor design and operation. Such polymerization reactors are often highly unstable and sensitive to temperature and mixing conditions (van der Molen and van Heerden, 1972). Over the past two decades, there have been some major modeling achievements including the determination of detailed reaction kinetics and the development of a host of phenomenological models for turbulent mixing effects on LDPE reactions (Villermaux and Blavier, 1984; Marini and Georgakis, 1984; Kiparissides et al., 1993; Tosun, 1992). Although using highly simplified descriptions of turbulent mixing, these phenomenological models are able to predict turbulent mixing effects in a qualitative manner through *ad hoc* assumptions of the mixing parameters. Most of these models apply multiple-stage or multiple-zone (e.g., Chan et al., 1993; Shirodkar and Tsien, 1986) methods to account for imperfect macromixing effects on polymerization processes by introducing mixing time scales at each stage or zone. Unfortunately, the mixing time scales in these models can only be determined by experimental or plant data and thus the models are unable to give any direct information on the implications of varying operating parameters, such as flow rate, feed temperature, and initiator injection location. For this reason, it is unlikely that such modeling approaches will produce any significant improvement for general reactor configurations. Some authors have concluded that axial mixing is negligible (e.g., Yoon and Rhee, 1985; Donati et al., 1982) for LDPE tubular reactors based on their large L/D ratio. However, since scalar mixing and chemical reactions are highly coupled, these conclusions may depend on whether scalar mixing is much slower than chemical reactions or how the initiator is introduced into the reactor. Furthermore, the effects of radial mixing on LDPE polymerization are seldom discussed due to the difficulties in closing the chemical reaction terms using traditional computational fluid dynamics (CFD) models for 2- or 3-D turbulent reacting flows (Fox, 1996). This work addresses these considerations from first principles by adopting a combined CFD and probability density function (PDF)

approach (Pope, 1985; Tsai and Fox, 1994; Pipino and Fox, 1994; Fox, 1996).

Recent developments in CFD have shown promise for simulating complex *nonreactive* flow systems, such as stirred tanks (Perng and Murthy, 1993; Bakker and Fasano, 1993), static mixers (Bakker et al., 1994), and two-phase flows (Lapin and Lübbert, 1994). These simulations are able to give reasonable approximations using moment methods to model the turbulent flow field. The well-known $k-\epsilon$ model (Launder and Spalding, 1974) and its renormalization-group (RNG) modification (Yakhot and Orzag, 1986) have been successfully applied in the fully turbulent regime. Their inability to cope with the near-wall zone and transitional flows is well understood and can be improved by incorporating wall functions or by using other more general models [e.g., Reynolds stress model (Rubinstein and Barton, 1990)]. However, moment methods encounter significant obstacles when applied to the scalar fields in turbulent *reacting* flows. Unlike the velocity field, the probability distribution of a scalar field is usually quite different from Gaussian (O'Brien, 1980). When chemical reactions are involved, modeling the higher-order moments of scalar fields can be extremely difficult. The arbitrariness of such modeling is illustrated in several papers (e.g., Heeb and Brodkey, 1990; Leonard et al., 1995). The presumed PDF method (Bilger, 1980; Jones and Whitelaw, 1982; Girimaji, 1991; Fox, 1996) presents a major step towards overcoming the moment closure problem. This method assumes a known probability density for the mixture fraction that depends only on its mean and variance, and uses chemical-equilibrium relationships between the mixture fraction and chemical reactants to derive the joint composition PDF for reactive scalars (Fox, 1996). Thus, the mean reaction rates for reactive scalars can be evaluated through an integral over the mixture fraction PDF. Although the chemical-reaction terms are closed in this formulation, the chemical-equilibrium assumption can produce significant errors for slow reactions. Moreover, the mixture fraction approach is restricted to nonpremixed initial conditions. Since LDPE polymerization includes a large number of reactions and a wide range of chemical-reaction rates, closing the mean reaction-rate terms using moment methods can result in large modeling errors. Furthermore, the temperature dependence of the reaction rates and their nonequilibrium nature also make the presumed PDF method inappropriate. In contrast, full PDF methods not only are capable of dealing with chemical-reaction terms without closures, they also can be applied to arbitrary initial conditions (O'Brien, 1980; Pope, 1985; Tsai and Fox, 1994). When combined with a CFD code for computing the turbulence field, this technique can be very efficient for simulating 2- and 3-dimensional turbulent reacting flows with acceptable computational costs. Turbulent reacting flow models are discussed in greater detail in the next section.

The joint composition PDF equations are formulated directly from the scalar transport equations without any closure assumptions. With the turbulence field found from a CFD code, transport of the full PDF in real space can be obtained from the joint composition PDF equation. Scalar means, variances, and mean reaction rates can then be evaluated from the joint composition PDF. However, the number of random variables in PDF methods increases linearly with the number of reacting scalars. A direct evaluation of the joint PDF (Jiang and O'Brien, 1991; Tsai and O'Brien, 1993) is thus intractable for inhomogeneous flows. Fortunately, several computationally efficient Monte-Carlo techniques have been developed by Pope (1981, 1985, 1994). Instead of evaluating the PDF directly, a set of Lagrangian notional particles is used to approximate PDF transport. With such techniques, the computational intensity increases only linearly with the number of reacting scalars, in contrast to an exponential increase when solving for the PDF directly. A Lagrangian composition PDF (LCPDF) code (Tsai and Fox, 1994), which is a modified version of Pope's Lagrangian velocity-composition PDF (PDF2DS) code (Pope, 1985), is adopted for this study. Although the LCPDF approach is ideally suited for dealing with reaction terms, the turbulent advection and diffusion terms still require modeling. The first term is associated with the large turbulence scales and is usually closed by the gradient-diffusion assumption. The second term, on the other hand, is associated with small scales and thus more difficult to model. In this work, the linear-mean-square-estimation (LMSE) (Dopazo, 1975) model is applied to solve the molecular diffusion terms. Further details on the numerical implementation are discussed in the next section.

Even with Monte-Carlo techniques, the computational expense for evaluating the chemical-reaction terms in a PDF simulation (or any other reacting flow simulation) still remains high. In order to further reduce the expense to a reasonable level, two strategies are used: simplified kinetics and chemical lookup tables. Although there is a substantial amount of literature available on the kinetics of LDPE polymerization (Lee and Marano, 1979; Goto et al., 1981; Zabisky et al., 1992), their ranges of validity are restricted to the experimental conditions for which they were derived. It is not the authors' intention to verify the correctness of the different kinetic schemes; instead, schemes have been chosen based on their consistency with tubular reactor data and computability. Two sets of temperature-dependent kinetics rate constants, one suggested by Goto et al. (1981) and the other by Lee and Marano (1979), are extensively examined with and without the quasi-steady-state assumption (QSSA) for a wide range of temperatures typical of industrial tubular LDPE reactors. A modified version of classical free-radical polymerization kinetics is adopted to reduce the total number of reacting scalars. The final kinetic scheme includes initiation, propagation, and termination by disproportion and chain transfer to monomer. Although it is well known that other mechanisms, such as β-scission and backbiting (i.e., transfer to polymer reactions), also contribute significantly to the weight- and number-distribution of polymer, those mechanisms have little or no net effect on the total monomer conversion and thus have not been included. (For a detailed LDPE kinetic model, see Kiparissides et al., 1993.) The polydispersity is found by the method of moments of the molecular-weight distribution (MWD) using QSSA for free-radicals and the long-chain hypothesis. However, even if the predicted values of the polydispersity may not be accurate due to the neglect of some mechanisms, they still serve as an indicator of final product quality under different operation conditions (Tosun, 1992). The kinetic scheme employed in this article involves six reactive scalars: initiator, monomer, the total dead polymer, the first and second moments of dead polymer, and temperature, and is discussed in detail in the

third section. A bifurcation and stability analysis of a similar kinetic scheme in a CSTR can be found in Marini and Georgakis (1984).

Since the large number of notional particles used in the Monte-Carlo simulation makes the direct numerical integration of the chemical-reaction terms computationally expensive, a chemical lookup table is used to store all possible changes of the composition variables over the (small) time step (e.g., Maas and Pope, 1992). This approach is possible whenever, as in the present study, the composition variables have bounded values. The composition values in each notional particle after the chemical-reaction step are found by interpolating from the chemical lookup table. This technique has been widely used in combustion studies, especially in the areas of PDF and flamlet research (e.g., Chen et al., 1989). In this work, the accuracy of this method is validated in the third section by comparison with results from the direct numerical integration of the chemical kinetic equations.

For industrial tubular LDPE reactors, it is well known that monomer conversion and polydispersity are strongly affected by mixing conditions and ethylene inlet temperature (Tosun, 1992; Kiparissides et al., 1993). A tubular LDPE reactor is usually controlled by adjusting the initiator feed stream to vary the reaction rate in order to avoid runaway polymerization that can cause ethylene decomposition. Therefore, in this study, the micromixing rate, inlet temperature, initiator feed rate, and initiator injection mode are chosen as the simulation parameters. In general, the results are found to be consistent with earlier studies using phenomenological mixing models and the plug-flow assumption (Goto, 1981; Kiparissides et al., 1993). The PDF simulations also give a clear picture of radial and axial mixing effects on LDPE polymerization in a tubular reactor that cannot be predicted by other models. For example, it is shown that radial inhomogeneity near the initiator injection point can lead to local hot spots and low initiator efficiency. The principal results from the simulation study are presented in the fifth section.

Turbulent Reacting Flow Models

The governing equations for the transport of reactive scalars in fluid flows with constant density can be written for the simplified LDPE kinetic scheme as (repeated indices imply summation)

$$\frac{\partial u_i}{\partial t} + u_j \frac{\partial u_i}{\partial x_j} = -\frac{1}{\rho}\frac{\partial p}{\partial x_i} + \frac{1}{\rho}\frac{\partial \tau_{ij}}{\partial x_j}, \qquad i = 1,2,3, \tag{1}$$

$$\frac{\partial \phi_k}{\partial t} + u_j \frac{\partial \phi_k}{\partial x_j} = D_{\phi_k}\nabla^2\phi_k + S_{\phi_k}(\phi),$$

$$\phi_k = \phi_I, \phi_M, \phi_R, \lambda_0, \lambda_1, \lambda_2 \text{ and } T \tag{2}$$

$$\nabla \cdot \boldsymbol{u} = 0, \tag{3}$$

where the viscous stress tensor is defined as

$$\tau_{ij} = \mu\left(\frac{\partial u_i}{\partial x_j} + \frac{\partial u_j}{\partial x_i}\right), \tag{4}$$

u_i is the fluid velocity, p the pressure, ρ the fluid density, ϕ_k the scalars carried by the fluid (i.e., molar concentrations, MWD moments, and temperature), D_{ϕ_k} the diffusivity of ϕ_k, ϕ the vector of ϕ_k, and $S_{\phi_k}(\phi)$ the homogeneous chemical production term discussed in the following section. In a CFD code, Eqs. 1–3 are rarely solved directly. Instead Reynolds averaging is invoked to decompose the fields into their mean and fluctuating components: $u_i = \langle u_i \rangle + u_i'$ and $\phi_k = \langle \phi_k \rangle + \phi_k'$.

In this work, the Reynolds-averaged, steady-state momentum equation is closed using the $k-\epsilon$ model. The details of this model can be found in Launder and Spalding (1974) and are not repeated here. The final model equations for mean velocities $\langle u_i \rangle$, turbulent kinetic energy (k), and dissipation rate (ϵ) read:

$$\frac{\partial \langle u_i \rangle}{\partial x_i} = 0 \tag{5}$$

$$\frac{\partial}{\partial t}\langle u_i \rangle + \frac{\partial}{\partial x_j}(\langle u_i \rangle \langle u_j \rangle) = \frac{\partial}{\partial x_j}\left(\nu \frac{\partial \langle u_i \rangle}{\partial x_j}\right) - \frac{1}{\rho}\frac{\partial \langle p \rangle}{\partial x_i} - \frac{\partial}{\partial x_j}\langle u_i' u_j' \rangle, \tag{6}$$

$$\frac{\partial}{\partial t}k + \frac{\partial}{\partial x_i}(\langle u_i \rangle k) = \frac{\partial}{\partial x_i}\left(\frac{\nu_t}{\sigma_k}\frac{\partial k}{\partial x_i}\right) + G_k - \epsilon, \tag{7}$$

and

$$\frac{\partial}{\partial t}\epsilon + \frac{\partial}{\partial x_i}(\langle u_i \rangle \epsilon) = \frac{\partial}{\partial x_i}\left(\frac{\nu_t}{\sigma_\epsilon}\frac{\partial \epsilon}{\partial x_i}\right) + C_1\frac{\epsilon}{k}G_k - C_2\frac{\epsilon^2}{k}, \tag{8}$$

where

$$\langle u_i' u_j' \rangle = \frac{2}{3}k\delta_{ij} - \nu_t\left(\frac{\partial \langle u_i \rangle}{\partial x_j} + \frac{\partial \langle u_i \rangle}{\partial x_i}\right), \tag{9}$$

$$G_k = \nu_t\left(\frac{\partial \langle u_j \rangle}{\partial x_i} + \frac{\partial \langle u_i \rangle}{\partial x_j}\right)\frac{\partial \langle u_j \rangle}{\partial x_i}, \tag{10}$$

and the turbulent viscosity is defined by

$$\nu_t = C_\mu \frac{k^2}{\epsilon}. \tag{11}$$

The choice of the model constants is addressed in the fifth section. The $k-\epsilon$ model equations are solved along with the log-law wall functions in order to resolve the strong anisotropic flow conditions in the boundary layer (Launder and Spalding, 1974).

The Reynolds-averaged mean scalar fields obey

$$\frac{\partial \langle \phi_k \rangle}{\partial t} + \langle u_j \rangle \frac{\partial \langle \phi_k \rangle}{\partial x_j} = -\frac{\partial}{\partial x_i}\langle u_i' \phi_k \rangle + D_{\phi_k}\frac{\partial^2 \langle \phi_k \rangle}{\partial x_j \partial x_j} + \langle S_{\phi_k}(\phi) \rangle. \tag{12}$$

In this expression, the turbulent flux term $\langle u_i' \phi_k \rangle$ is closed by invoking the gradient-diffusion assumption:

$$\langle u_j' \phi_k \rangle = -\Gamma_T \frac{\partial \langle \phi_k \rangle}{\partial x_j}. \tag{13}$$

Here local isotropy is implied by the use of the scalar coefficient Γ_T. In a more general model, Γ_T can be treated as a tensor (Rogers et al., 1989). In most CFD codes, Γ_T is modeled by $C_\mu(k^2/\epsilon)/\sigma_\phi$, which resembles the model for turbulent viscosity (Eq. 11) where σ_ϕ is the turbulent Schmidt number and has a value near 0.7 (Launder and Spalding, 1974).

In order to solve Eq. 12, the unclosed chemical reaction term must be expressed in terms of the mean scalar variables. This presents a very challenging problem. For example, in order to obtain the evolution equation for the initiator mean concentration $\langle \phi_I \rangle$ the following term must be closed:

$$\langle S_{\phi_I}(\phi) \rangle = \langle k_d(T) \phi_I \rangle. \tag{14}$$

Since k_d is a function of temperature, which is also a turbulent quantity, in order to solve for $\langle \phi_I \rangle$, $\langle S_{\phi_I}(\phi) \rangle$ must be expressed in terms of $k_d(\langle T \rangle)$ and $\langle \phi_I \rangle$. Unfortunately,

$$\langle k_d(T) \phi_I \rangle \neq k_d(\langle T \rangle) \langle \phi_I \rangle, \tag{15}$$

nor is there any other simple relation that is valid in general. For example, the predictions of even the most sophisticated moment closure (Heeb and Brodkey, 1990) for the relatively simple two-step consecutive (or competitive) reaction are unsatisfactory. Thus, given the complexity of the LDPE polymerization, moment closure approaches are likely to be inadequate.

Another difficulty in handling Eq. 2 is the choice of micromixing time scale. For example, the decay rate of an inert scalar variance can be written as (Fox, 1995),

$$\frac{\partial \langle \phi'^2 \rangle}{\partial t} + \langle u_j \rangle \frac{\partial \langle \phi'^2 \rangle}{\partial x_j} = -\frac{\partial}{\partial x_j} \langle u_j' \phi'^2 \rangle - 2\langle u_j' \phi \rangle \frac{\partial \langle \phi \rangle}{\partial \langle x_j \rangle} - 2\left\langle D_\phi \frac{\partial \phi'}{\partial x_j} \frac{\partial \phi'}{\partial x_j} \right\rangle. \tag{16}$$

The turbulent flux term $\langle u_j' \phi'^2 \rangle$ is again closed by invoking the gradient-diffusion assumption. The last term on the right-hand side is the scalar dissipation term. The usual assumption invokes the eddy breakup model:

$$2\left\langle D_\phi \frac{\partial \phi'}{\partial x_j} \frac{\partial \phi'}{\partial x_j} \right\rangle = \frac{C_\phi}{\tau_\phi} \langle \phi'^2 \rangle, \tag{17}$$

where C_ϕ is a model constant and τ_ϕ is often referred to as the micromixing time. The micromixing time must be related to the turbulent time scales. The most commonly used turbulent time scales are k/ϵ, $(\nu/\epsilon)^{1/2}$, and $d/\sqrt{k}$. The first is used when scalar mixing is dominated by large-scale motions (e.g., jet stirred mixer with jet diameter close to the mixer diameter), the second is used when scalar mixing is generated by small-scale motions (e.g., a large mixer with one reactant injected through small feed tubes), and the last is commonly used for fully developed pipe flows. A complete model should also include nonequilibrium effects (e.g., Pipino and Fox, 1994; Fox, 1995; Tsai and Fox, 1996).

The micromixing time scale is usually included in LDPE mixing models by introducing a mixing time constant, which is adjusted according to different operation conditions. Unfortunately, such approaches are far from reality and provide little insight into the interactions between turbulence and the polymerization reaction. Once the operating conditions are changed, the mixing time constant can change completely. The plug-flow model (e.g., Kiparissides et al., 1993) neglects micromixing by assuming $\langle \phi'^2 \rangle = 0$, as well as "mesomixing" by assuming that the turbulent Peclet number $(\langle u \rangle L\epsilon/k^2)$ is infinite, and only considers the overall time constant $L/\langle u \rangle$. In the infinite Peclet number limit, the turbulent flux and molecular diffusion terms are negligible, and Eq. 12 becomes

$$\frac{\partial \langle \phi_k \rangle}{\partial t} + \langle u_j \rangle \frac{\partial \langle \phi_k \rangle}{\partial x_j} = S_{\phi_k}(\langle \phi \rangle). \tag{18}$$

The plug-flow model then follows by assuming that $\langle u_j \rangle$ is constant and nonzero only in the direction of the flow. The plug-flow assumption may be invalid when predicting the initiator efficiency since the reaction time scales are much smaller than the mixing time scales at high temperature (i.e., $\langle \phi^2 \rangle \neq 0$). Indeed, because the initiator is usually injected through a high-thrust nozzle, the reaction can be highly localized and very sensitive to temperature. In this case, radial mixing cannot be neglected as shown in the fifth section.

Similar problems also plague the presumed PDF method. This method solves Eqs. 12 and 16 for the mean and variance of the mixture fraction ($\langle S_{\phi_k}(\phi) \rangle = 0$) and then assumes, for example, that it has a beta PDF. The relationships between reactive scalars and the mixture fraction are derived by assuming instantaneous chemical equilibrium (mixed is burnt) (Fox, 1996). Although this model is able to account for the micromixing effects, the instantaneous chemical equilibrium assumption will produce significant errors when a chemical reaction is irreversible or has a finite reaction rate. This has particularly significant consequences for the LDPE reactor. Since the initiator is injected at relatively low temperatures, initiator and ethylene will be well mixed before chemical reaction starts. With the presumed PDF model, this will result in an overprediction of initiator efficiency, giving results similar to the plug-flow model that ignores mixing effects.

The only technique that can avoid all of these shortcomings is the full PDF method (O'Brien, 1980; Pope, 1985; Tsai and Fox, 1994). Unlike the presumed PDF method, the full PDF method directly solves the PDF transport equation for reactive scalars, and thus, the instantaneous chemical equilibrium assumption is not required. In this study, PDF simulations are performed using a Monte-Carlo algorithm that represents the joint PDF by an ensemble of Lagrangian notional particles moving in the computational domain (Tsai and Fox, 1994). Each of the particles obeys a set of stochastic differential equations (SDEs) that mimic the PDF transport in physi-

cal and phase space. Before the SDEs are fomulated, the PDF balance equation is derived from the Navier–Stokes equation and the conservation equations for passive scalars. Detailed descriptions of PDF methods can be found in O'Brien (1980) and Pope (1985). Here, only the final formulation employed in this study is outlined.

The evolution equation for the joint composition PDF, $f_\phi(\psi; x, t)$, can be written as

$$\rho\frac{\partial f_\phi}{\partial t}+\rho\langle u_j\rangle\frac{\partial f_\phi}{\partial x_j}+\frac{\partial}{\partial\psi_k}\left[\rho S_{\phi_k}(\psi)f_\phi\right]=-\rho\frac{\partial}{\partial x_j}\langle u_j'\mathfrak{F}\rangle - \frac{\partial}{\partial\psi_k}\left[\left\langle\frac{\partial}{\partial x_i}\left(\rho D_{\phi_k}\frac{\partial\phi_k}{\partial x_i}\right)\middle|\psi\right\rangle f_\phi\right], \quad (19)$$

where ψ is the composition phase variable, $\mathfrak{F}$ the fine-grained density function defined as $\delta(\phi-\psi)$ (O'Brien, 1980), and the term of the form $\langle..|.\rangle$ on the righthand side is the conditional expectation of molecular diffusion (Pope, 1985), which is an unknown function of ψ. A remarkable feature of the PDF approach can be seen by observing that all of the terms on the lefthand side of Eq. 19 are closed. These terms include transport in physical space by the mean velocity, and transport in composition space by chemical reactions. This feature gives a great advantage to the PDF method over traditional CFD approaches. Nevertheless, the two conditional expectation terms on the righthand side of Eq. 19, representing transport in velocity space by turbulent fluctuations and molecular mixing still require modeling. The first is modeled as in Eq. 13:

$$\langle u_j'\mathfrak{F}\rangle=-\Gamma_T\frac{\partial f_\phi}{\partial x_j}. \quad (20)$$

The second is closed by the well-known LMSE model (Dopazo, 1975). Assuming equal diffusivity, the LMSE model can be expressed by

$$\left\langle\frac{\partial}{\partial x_i}\left(\rho D_{\phi_k}\frac{\partial\phi_k}{\partial x_i}\right)\middle|\psi\right\rangle=\frac{\rho}{2\tau_\phi}C_\phi(\psi_i-\langle\phi_i\rangle), \quad (21)$$

where C_ϕ is an empirical constant and τ_ϕ the micromixing time scale, both of which depend on the choice of mixing rate model.

Since the dimensions of Eq. 19 increase linearly with the number of reactive scalars, the direct computation of $f(\phi)$ is intractable. Instead, a set of Lagrangian SDEs is formulated. The relationship between the SDEs and Eq. 19 is derived using the Fokker–Plank equation (Gardiner, 1985). The details can be found elsewhere (Pope, 1985) and are not repeated here. The resultant SDE for the position of a Lagrangian particle reads

$$d\boldsymbol{x}=[\langle\boldsymbol{u}\rangle+\nabla\Gamma_T/\rho]_{x(t)}dt+[2\Gamma_T/\rho]^{1/2}_{x(t)}d\boldsymbol{W}(t), \quad (22)$$

where the subscript $\boldsymbol{x}(t)$ denotes the spatial location where the coefficient is evaluated. In the Monte-Carlo simulation, $d\boldsymbol{W}(t)$ is approximated by $\boldsymbol{\xi}(\Delta t)^{1/2}$ where $\boldsymbol{\xi}$ is a standardized joint normal random vector. Likewise, the scalar values in a particle obey

$$\frac{d\psi_i}{dt}=-\frac{1}{2\tau_\phi}C_\phi(\psi_i-\langle\phi_i\rangle)_{x(t)}+S_{\phi_k}(\psi). \quad (23)$$

Note that in general τ_ϕ will also be a function of the particle location $\boldsymbol{x}(t)$, thereby coupling Eq. 23 to Eq. 22. Similarly, the SDEs are coupled to the velocity field (Eqs. 5–8) through the coefficients (e.g., $\langle u\rangle$ and Γ_T). The reaction rate, $S_{\phi_k}(\boldsymbol{\psi})$ is a function only of the local composition vector $\boldsymbol{\psi}$, and thus can be stored in a chemical lookup table described in the next section. More details concerning the numerical implementation of the Monte-Carlo simulations can be found in Tsai and Fox (1994, 1995).

LDPE Polymerization Kinetics

The kinetic model employed in this work is a modified form of free-radical addition polymerization with chain transfer to monomer, and with disproportion as the only chain termination mechanism (i.e., transfer to polymer has been neglected). The adopted kinetic scheme is as follows:

Initiation

$$I\xrightarrow{k_d}2A \quad (24)$$

$$I\xrightarrow{k_x}X \quad (25)$$

$$A+M\xrightarrow{k_i}R_1. \quad (26)$$

Propagation

$$M+R_n\xrightarrow{k_p}R_{n+1}. \quad (27)$$

Termination

$$R_n+R_m\xrightarrow{k_{td}}P_n+P_m. \quad (28)$$

Chain transfer to monomer

$$R_n+M\xrightarrow{k_{trm}}P_n+R_1. \quad (29)$$

In Eq. 24 initiator (I) breaks down to produce the initiator radical A. The inert product X, which was suggested by Goto et al. (1981), results from initiator deactivation. The initiator radical reacts with the monomer (M) in Eq. 26 with a monomer activation rate constant k_i to produce growing polymer of unit length (R_1). Chain propagation occurs by the addition of monomer to growing polymer of length n (R_n) in Eq. 27 with a polymerization rate constant k_p. Dead polymer chains (P_n) are created in Eq. 28 with a termination rate constant k_{td}, and finally the chain transfer to monomer has a rate constant k_{trm} and produces dead polymer of length n and growing polymer of length 1.

Defining the total radical polymer and total dead polymer by $R=\sum_{n=1}^{\infty}$, R_n and $P=\sum_{n=1}^{\infty}P_n$, respectively, and applying

the moments of MWD, the homogeneous kinetic equations follow from Eqs. 24–29:

$$S_{\phi_I}(\phi) = -k_d\phi_I - k_x\phi_I, \tag{30}$$

$$S_{\phi_A}(\phi) = 2k_d\phi_I - k_i\phi_A\phi_M, \tag{31}$$

$$S_{\phi_R}(\phi) = k_i\phi_A\phi_M - 2k_t\phi_R^2, \tag{32}$$

$$S_{\phi_M}(\phi) = -k_i\phi_A\phi_M - k_p\phi_R\phi_M - k_{trm}\phi_R\phi_M, \tag{33}$$

$$S_{\lambda_0}(\phi) = k_{trm}\phi_M\phi_R + 2k_t\phi_R^2, \tag{34}$$

$$S_{\lambda_1}(\phi) = k_i\phi_A\phi_M + (k_{trm} + k_p)\phi_M\phi_R, \tag{35}$$

and

$$S_{\lambda_2}(\phi) = k_i\phi_A\phi_M + (k_{trm} + k_p)\phi_M\phi_R + 2k_p\phi_M\mu_1, \tag{36}$$

where

$$\mu_1 = \frac{k_i\phi_A\phi_M + (k_{trm} + k_p)\phi_M\phi_R}{k_{trm}\phi_M + 2k_t\phi_R}. \tag{37}$$

Note that these expressions are coupled to the energy balance through the rate constants as discussed below.

The number- and weight-averaged degree of polymerization are calculated using the following relations:

$$DP_n = \frac{\lambda_1}{\lambda_0}, \tag{38}$$

$$DP_w = \frac{\lambda_2}{\lambda_1}, \tag{39}$$

The polydispersity ratio Z_p is calculated from its definition:

$$Z_p = \frac{DP_w}{DP_n}. \tag{40}$$

The kinetic equations can be further simplified by invoking the quasi-steady-state approximation (QSSA) and long-chain hypothesis that eliminate Eqs. 31 and 32, and relating the free-radical to reactant concentrations:

$$\phi_A = \frac{2k_d\phi_I}{k_i\phi_M} \tag{41}$$

and

$$\phi_R = \left(\frac{k_d\phi_I}{k_t}\right)^{1/2}. \tag{42}$$

These assumptions have been validated for the plug-flow model as discussed below.

Two sets of reaction rate constants have been investigated. The first set is taken from Goto et al. (1981):

$$k_d(T, P_{\text{atm}}) = 6.639\times10^{15}\exp\left(\frac{-1.876\times10^4}{T} - \frac{2.5P_{\text{atm}}}{82.06T}\right), \tag{43}$$

$$k_x(T, P_{\text{atm}}) = 2.04\times10^{28}\exp\left(\frac{-3.42\times10^4}{T}\right), \tag{44}$$

$$k_p(T, P_{\text{atm}}) = 1.564\times10^5\exp\left(\frac{-5.29\times10^3}{T} + \frac{19.7P_{\text{atm}}}{82.06T}\right), \tag{45}$$

$$k_{td}(T, P_{\text{atm}}) = 8.333\times10^4\exp\left(\frac{-1.833\times10^3}{T} - \frac{13.0P_{\text{atm}}}{82.06T}\right), \tag{46}$$

$$k_{trm}(T, P_{\text{atm}}) = 4.861\times10^5\exp\left(\frac{-7.08\times10^3}{T} - \frac{4.4P_{\text{atm}}}{82.06T}\right), \tag{47}$$

where P_{atm} is the operating pressure in units of atmospheric pressure. In this study, a value of 2,150 atm is employed (Smit, 1992). The second set was derived by Lee and Marano (1979):

$$k_p(T, P_{\text{atm}}) = 5.887\times10^4\exp\left(\frac{-3.572\times10^3}{T} + \frac{23.72P_{\text{atm}}}{82.06T}\right), \tag{48}$$

$$k_{td}(T, P_{\text{atm}}) = 1.075\times10^6\exp\left(\frac{-1.5\times10^2}{T} + \frac{14.49P_{\text{atm}}}{82.06T}\right), \tag{49}$$

and

$$k_{trm}(T, P_{\text{atm}}) = 5.823\times10^2\exp\left(\frac{-5.561\times10^3}{T} + \frac{20.65P_{\text{atm}}}{82.06T}\right), \tag{50}$$

It should be noted that both sets of rate constants have the same expression for k_d (Eq. 43) based on *di-tert-butyl peroxide*, which is effective over a wide range of desirable polymerization temperatures. The initiator consumption rate constant k_x appears exclusively in the study of Goto et al. (1981). Without k_x, the kinetic scheme will produce excessively high polymer propagation due to the high value of k_p/k_t (Zabisky et al., 1992).

Since all rate constants are functions of temperature, an enthalpy balance must be employed. Assuming that the major heat release is from the propagation step (Kiparissides et al., 1993), one obtains

$$S_T(\phi) = \left(\frac{\Delta H}{\rho C_p}\right)k_p\phi_M\phi_R, \tag{51}$$

where ρ is the density of the reaction mixture, ΔH the enthalpy change for monomer propagation, and C_p the heat

capacity. Since our current implementation of the LCPDF code is unable to predict the influence of the chemical reactions on the flow field, it is necessary to assume constant physical properties for the reaction mixture in the reaction zone. The values used by Smit (1992) are employed: $\rho = 444$ kg/m^3, $\Delta H = 94{,}893$ J/mol, $C_p = 2{,}510$ J/kg·K. However, in reality, both ρ and viscosity increase with monomer conversion, but since the monomer conversion is relatively low for the simulations in this study, the effects are limited. The details are discussed in the fourth section.

As noted in the Introduction, more detailed kinetic schemes (e.g., Goto et al., 1981; Kiparissides et al., 1993) include termination by combination, chain transfer to solvent, chain transfer to polymer, backbiting, and β-scission. The kinetic scheme adopted here is a compromise between numerical tractability and usefulness for capturing mixing effects on initiator efficiency. The simplified kinetics are able to capture the effects of turbulent mixing on the yield since all the kinetic steps that change the monomer conversion have been included. The omitted kinetic steps only affect interpolymer distributions (e.g., λ_1 and λ_2). Note also that the QSSA can affect the monomer conversion significantly if Goto's kinetic rate constants are employed. This effect is examined in detail below.

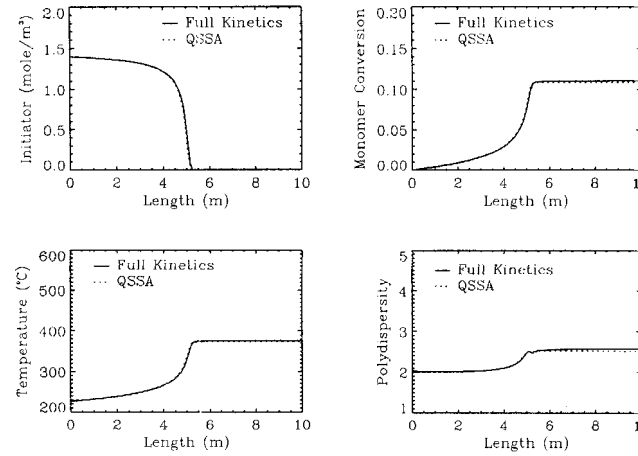

Figure 1. Axial profiles of initiator concentration, monomer conversion, temperature and polydispersity in an adiabatic plug-flow reactor with mean velocity equal to 1.0 m/s using rate constants of Lee and Marano (1979) with initial initiator and monomer concentrations equal to 1.4 and 15,856 mol/m^3, respectively, and initial temperature of 227°C.

Validation of QSSA and comparison of kinetic rate constants

Generally speaking, the accuracy of the QSSA depends on the temperature. When the temperature is low, the relatively high k_t and low k_d assure a rapid consumption of free-radicals, and therefore R can be correctly approximated by QSSA. Here, validation of the QSSA is performed by employing the full kinetics (Eqs. 30–51) with R given by Eq. 32 (full kinetics) and Eq. 42 (QSSA) for an adiabatic plug-flow reactor. A comparison of the rate constants by Goto et al. (1992) and Lee and Marano (1979) has also been conducted. It should be noted that k_x is essential for the kinetics of Goto et al. Without this extra term, Goto's rate constants will predict unphysically high values of monomer conversion due to its high values of k_p/k_t (Zabisky et al., 1992).

Shown in Figures 1 and 2 are the predictions of the evolutions of initiator, monomer conversion, temperature, and polydispersity with and without the QSSA using Lee and Marano's rate constants at $T = 227$°C and 327°C, which covers the temperature range of the simulations in this study. In the figures, initiator and monomer have initial concentrations of 1.4 mole/m^3 and 15,856 mole/m^3, respectively (the initial initiator concentration is equal to the highest feed concentration used in the full PDF simulations). The results are virtually identical with and without the QSSA except for the polydispersity, which only has an error less than 2% in both cases. Other initial concentrations of initiator produce similar results (not shown).

Interestingly, the rate constants of Goto et al. (1981) produce completely different behavior. As shown in Figures 3 and 4, the QSSA produces an error of more than 100% for monomer conversion at initial temperatures of 227°C and 277°C. Similar errors persist even at a temperature as low as 150°C. The error comes from the fact that Goto's kinetics require the extra initiator deactivation rate constant k_x to correctly predict the polymer propagation rate. The QSSA, which invokes $R = (k_d \phi_I / k_t)^{1/2}$, is no longer appropriate. However, no definitive conclusion about which rate constants are the "best" can be drawn from these comparisons since both sets provide satisfactory results in the original articles. Therefore, Lee and Marano's rate constants are adopted in this work because of their consistency with other tubular reactor studies (Zabisky et al., 1992) and with the QSSA.

Chemical lookup table

Although the chemical reaction terms are treated exactly in the PDF formulation, a direct evaluation of these terms is still prohibitively expensive for complex kinetic schemes. A typical simulation in this study involved approximately 100,000 particles in the computational domain; therefore, a direct in-

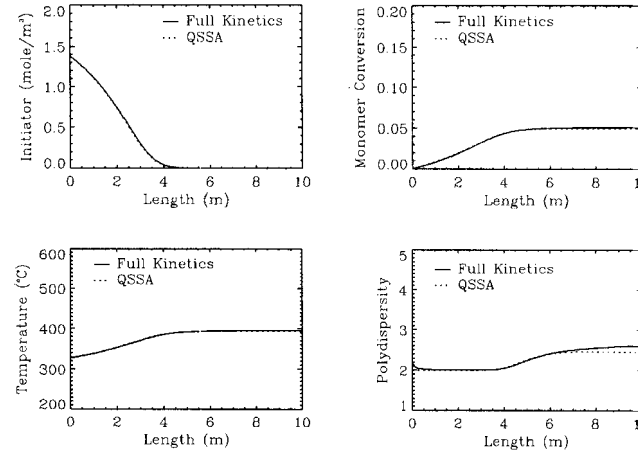

Figure 2. Same as in Figure 1, but with initial temperature of 327°C.

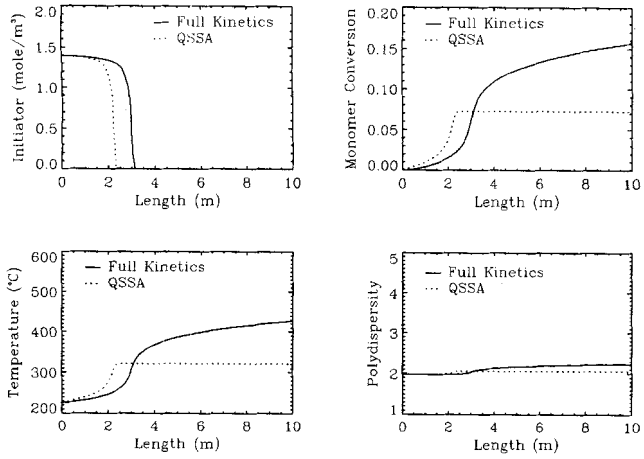

Figure 3. Axial profiles of initiator concentration, monomer conversion, temperature and polydispersity in adiabatic plug-flow reactor with mean velocity equal to 1.0 m/s using rate constants of Goto et al. (1981) with initial initiator and monomer concentrations equal to 1.4 and 15,856 mol/m^3, respectively, and initial temperature of 227°C.

tegration of the chemical reaction terms in Eq. 23 would require solving a stiff system of ODEs (Eqs. 30–51) approximately 100,000 times at each time step, which is impractical in view of the computational costs. However, because chemical species always have bounded values, it is possible to generate a chemical lookup table that stores the incremental changes over a fixed time step for all scalars within the bounded domain (Chen et al., 1989; Maas and Pope, 1992). The chemical reaction terms in Eq. 23 are evaluated during the simulation by interpolating from the chemical lookup table. Our experience has shown that lookup tables can decrease computational costs by as much as 95% as compared to direct integration.

For the chemical kinetics adopted in this study, the lookup table consists of three independent variables, ϕ_I, ϕ_M, and T, and six dependent variables, ϕ_I, ϕ_M, λ_0, λ_1, λ_2, and T, as

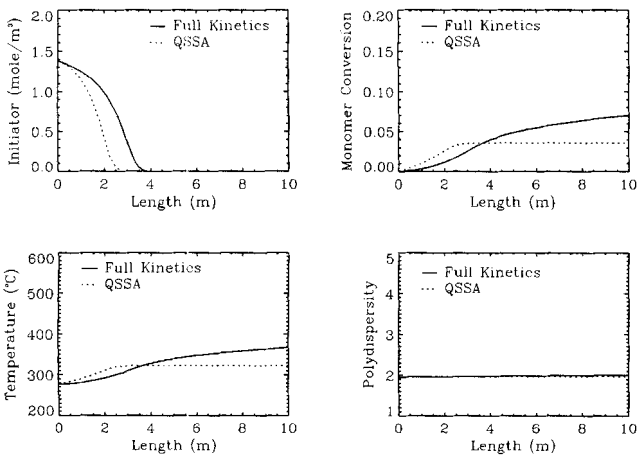

Figure 4. Same as in Figure 3, but with an initial temperature of 277°C.

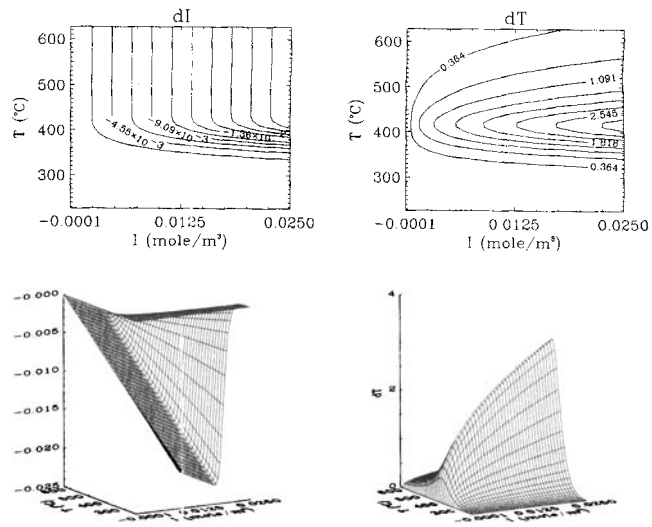

Figure 5. Change in temperature (dT) (right) and initiator (dI) (left) over one time step ($\Delta t = 3.85 \times 10^{-4}$ s) as a function of initiator concentration (I) and temperature (T) with a fixed monomer concentration of 14,000 mol/m^3.

Note that in the PDF simulation, a notional particle would step along a trajectory in $T-I$ phase space ($I \rightarrow I + dI$, $T \rightarrow T + dT$) at each time step, followed by a mixing step. In a plug-flow reactor, the mixing step is absent and the notional particle steps along a trajectory in $T-I$ phase space that can be found directly from the plots of dT and dI.

derived from Eqs. 30–51 after invoking the QSSA. The table thus contains 6×40^3 real numbers stored at a total of 40^3 grid locations. As an example, Figure 5 shows the increments of initiator (dI) and temperature (dT) as functions of initiator concentration (I) and temperature (T) with the monomer concentration fixed at 14,000 mole/m^3 and for a time step of 3.85×10^{-4} s, which was determined by the numerical stability of the flow field. The peak values along the temperature axis are correctly captured within the resolution of the lookup table. The incremental values for each node in the lookup table were found by numerical integration using the ODE solver LSODAR (Petzold and Hindmarsh, 1987). The accuracy of the lookup table was validated by checking the interpolated values against direct numerical integration of Eqs. 30–51 at randomly selected coordinates in composition space. The error was found to be within 0.1%. More details concerning chemical lookup tables can be found in Maas and Pope (1992).

LDPE Tubular Reactor Simulations

A plant-scale, tubular LDPE reactor has a long preheating section to provide adequate heat exchange in order to increase the temperature of ethylene to initiate reaction. In the PDF simulations, the turbulent flow field starts at the end of the preheating section and is thus assumed to be fully developed. The flow rate of ethylene is set at 11.0 kg/s (Kiparissides et al., 1993). Since, in comparison, the initiator injection rate is relatively small (typically at a ratio of 1:10,000 to ethylene), the flow field is assumed to be unaffected by initiator injection.

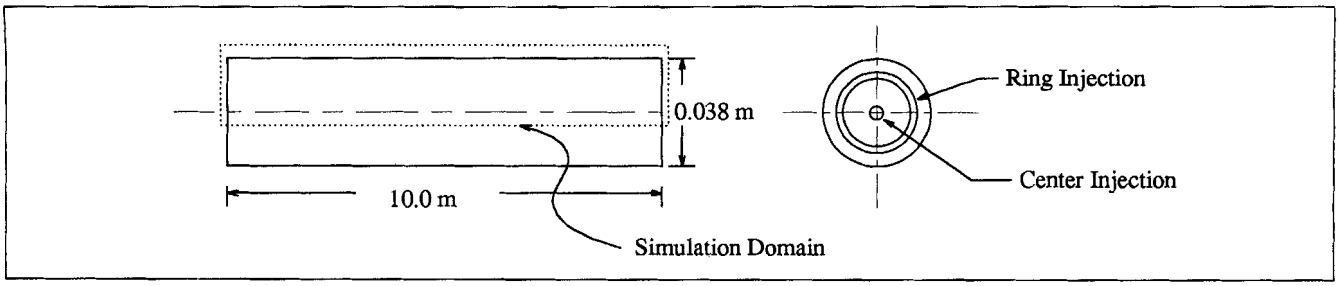

Figure 6. Top and end view of the LDPE tubular reactor.

The simulation domain only includes the top half of the reactor (enclosed by the dotted line) due to symmetry. Three modes of initiator injection have been simulated: center, ring, and uniform. For the latter, initiator is uniformly distributed over the reactor cross section.

Earlier plug-flow reactor studies have shown that the reaction goes to completion over a relatively short distance in a tubular reactor, usually within one-tenth of the total length. This suggests that heat removal is unimportant during the reaction process, acting principally to decrease the temperature of the reaction mixture to the quenching temperature before the next injection point. In this work, only one reaction zone is simulated. A top and side view of the simulation domain is shown in Figure 6 with a total length of 10 m (about one-tenth of a standard plant-scale tubular LDPE reactor). The length was chosen so that the simulation would capture the entire reaction zone.

As mentioned previously, the flow field is assumed to be unaffected by changes in the fluid properties. In the LDPE reactor, only fluid density and viscosity variations could affect the flow field. However, since the density and viscosity of ethylene and LDPE vary only slightly in the temperature range between 227°C and 327°C ($\leq 5\%$, Kiparissides et al., 1993), and the flow rate is very high, the effects of such small variations in fluid density and viscosity should be limited. Moreover, since the flow is fully turbulent, molecular coefficients such as viscosity and diffusivity will have minimal effect on the Reynolds-averaged flow field. Technically, it is possible to include fluid density variations in the reactor simulations by passing the mean density field computed by the LCPDF code back to FLUENT and iterating until statistical convergence is achieved (Roekaerts, 1991). Variable-density simulations will be reported in a future communication.

The empirical constants for the $k-\epsilon$ model used in this work (Eqs. 6-8) have the following values (Launder and Spalding, 1974):

$$C_1 = 1.44, \quad C_2 = 1.92, \quad C_\mu = 0.09, \quad \sigma_k = 1.0, \quad \sigma_\epsilon = 1.3, \qquad (52)$$

and generate a good fit to experimental data (Laufer, 1954; Hrenya et al., 1995) for fully developed turbulent pipe flow. Figure 7 shows the predicted velocity mean and rms radial profiles. The predicted centerline k and ϵ values are 1.37 m^2/s^2 and 80.8 m^2/s^3, respectively. The Reynolds number is approximately 50,000 based on the mean velocity and tube diameter. The computational domain has an orthogonal grid of size 199×99 with a uniform grid spacing in the radial direction. Although the velocity field is assumed to be fully developed (i.e., independent of axial location), the scalar field is evolving along the reactor, therefore, a stretched grid spacing is used in the axial direction with denser grids near the initiator injection point. After the turbulent velocity field is obtained, the mean velocity $\langle u_i \rangle$, turbulent kinetic energy k, and dissipation rate ϵ fields are input into the LCPDF code for evaluating the coefficients in Eqs. 22 and 23.

Several operating parameters can be varied for the LCPDF simulation, including the inlet monomer temperature, the inlet initiator concentration, and the monomer flow rate. In a plant-scale reactor, these variables are usually used as control parameters. A typical LDPE tubular reactor has a very long preheating section to increase the ethylene to a predetermined feed temperature. The choice of the latter not only depends strongly on the type of initiator employed, but also has a significant effect on the final quality of polymer. The reaction is carefully controlled by the rate of initiator injection to avoid runaway reactions. In a tubular LDPE reactor, the flow rate (Reynolds number) is the primary factor in determining the mixing rate. In this study, the effect of mixing rate is investigated by varying C_ϕ in Eq. 23. As a result, there are four operating parameters in the simulations: inlet monomer temperature, micromixing rate, initiator concentration (or injection rate), and initiator injection mode. The last two parameters require further explanation.

In most plant-scale reactors, in order to maximize the initiator efficiency, the injection nozzle is specially designed for a high mixing rate. The nozzle geometry is usually very complicated and involves small jets at length scales that are much

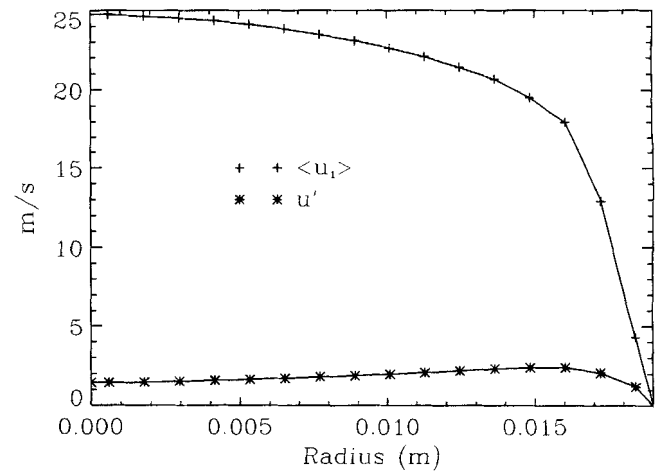

Figure 7. Mean ($\langle u_1 \rangle$) and rms (u') radial profiles of axial velocity.

smaller than the integral scale of turbulent pipe flow. A detailed CFD simulation of the injection nozzle is thus impractical (if not impossible). Therefore, since near the nozzle the local micromixing rate is very high ($59\ s^{-1} < 1/\tau_\phi < 2{,}200\ s^{-1}$), the inlet temperature is relatively low (i.e., the reaction rate is low: $k_d = 9.06\ s^{-1}$ at 277°C), and the initiator flow rate is small compared to the mean flow rate (ratio $\approx$ 0.0002 to 0.0006), it is reasonable to assume that the initiator and monomer are locally well mixed in the computational cell containing the injector. For the simulations, this implies that fixing the flow rate of the initiator and varying its concentration is equivalent to fixing the initiator concentration and varying its flow rate. With this assumption, the initial concentration of initiator in the injection cell is determined by the cell size and initiator flow rate. In this study, the inlet initiator concentration and temperature before injection are set at 250 mol/m^3 and 77°C, respectively.

The final parameter is the initiator injection mode and refers to the manner with which the initiator is introduced at the inlet (see Figure 6). For example, it is possible to introduce initiator only at the centerline of the reactor, or to inject it uniformly across the reactor cross section. In terms of the simulation, this parameter translates into the number and distribution of injection cells. Since we have assumed the flow field to be 2- and 3-D effects such as off-center injection cannot be simulated with the current code. Nevertheless, as seen in the sixth section, the qualitative effects of the initiator injection mode can be investigated and are shown to have a significant influence on reactor performance. Since the initiator flow rate is very small compared to the monomer, the premixed temperature is assumed to be the same as the initial monomer temperature and the initiator concentration has values of 2.73 mol/m^3, 0.257 mol/m^3, and 0.05 mol/m^3, respectively, for center-, ring- and uniform-mode injection with an initiator-to-monomer flow rate ratio of 0.0002.

These four operating parameters completely determine the initiator efficiency in the PDF simulations. Since they are strongly coupled, the effect of varying one parameter depends on the values of the other three parameters. A thorough study should thus cover the 4-dimensional parametric space. Unfortunately, although possible, this is computationally expensive and is unnecessary in order to gain a qualitative understanding of turbulent mixing effects in the reactor. The simulation results that are most essential for understanding the behavior and improving the design and control of tubular LDPE reactors are presented in the next section.

Results and Discussion

It is well known that the polymerization is highly sensitive to temperature fluctuations, or so-called hot spots (Smit, 1992). Poor local mixing can result in several undesirable effects: (1) the initiator burns out without transforming monomer into polymer; (2) the high temperature causes the decomposition of monomer, producing pure carbon and shutting down the reactor; (3) local hot spots can create transient instability, which is undesirable for reactor startup, process control, and product quality. According to our earlier studies (Tsai and Fox, 1994; Pipino and Fox, 1994; Fox, 1995), the value of the turbulent mixing parameter C_ϕ is of fundamental importance for accurate simulations. Assuming a fully developed velocity spectrum, a set of equations can be formulated for the evolution of scalar micromixing time scale (Fox, 1995; Tsai and Fox, 1996), thereby fixing the value of C_ϕ without recourse to empirical parameters. The application of this detailed model requires an accurate estimation of the initial length scales of the initiator and the local length scales of velocity field. This information is not available for the injector region of the LDPE reactor. Thus, in this study, a simple estimation of the turbulence integral scale is made based on the reactor diameter. The standard expression for the micromixing rate ($1/\tau_\phi$) for fully developed turbulent pipe flow has the form $C_\phi\sqrt{2k}/d$ (Tsai and Fox, 1994), where d is the tube diameter, and C_ϕ is near unity for inert scalars (Béguier et al., 1978). For the present reactor this yields $1/\tau_\phi \approx C_\phi \times 43.6\ s^{-1}$ (centerline value).

Effect of micromixing

Figure 8 presents axial profiles of the radially averaged fields for initiator, temperature, monomer conversion, and polydispersity for $C_\phi = 2.0$, 1.5, and 1.0 with the initiator injected at the centerline (Figure 6) and an inlet monomer temperature of 252°C. Since C_ϕ determines the relative rate of micromixing, higher C_ϕ yields higher monomer conversion, a higher final reactor temperature, and lower polydispersity. These conclusions are in agreement with experimental studies of the effect of mixing in LDPE reactors (van der Molen and van Heerden, 1972). Figure 8a shows how initiator is consumed along the reactor. At lower micromixing rates, more initiator is consumed right after the injection point. This phenomenon not only reduces the monomer conversion rate, but can also trigger local hot spots that may cause a thermal runaway reaction leading to monomer decomposition. Figure 9 presents hot-spot distributions computed from the temperature pdf for $C_\phi = 1.0$ and 1.5. Each black dot in the figures indicates the location of the highest particle temperature occurring at each time step for the last 1,000 time steps during

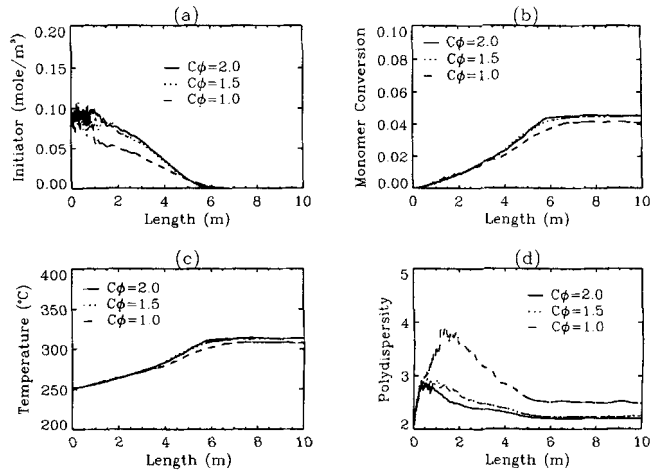

Figure 8. Radially averaged quantities vs. reactor length at different values of C_ϕ with center-mode injection, an inlet monomer temperature (T_{inlet}) of 252°C, and an initiator-to-monomer flow rate ratio (F_I) of 0.0004.

The final values of λ_1 are 1,940 mol/m^3 ($C_\phi = 2.0$), 1,880 mol/m^3 ($C_\phi = 1.5$), and 1,840 mol/m^3 ($C_\phi = 1.0$).

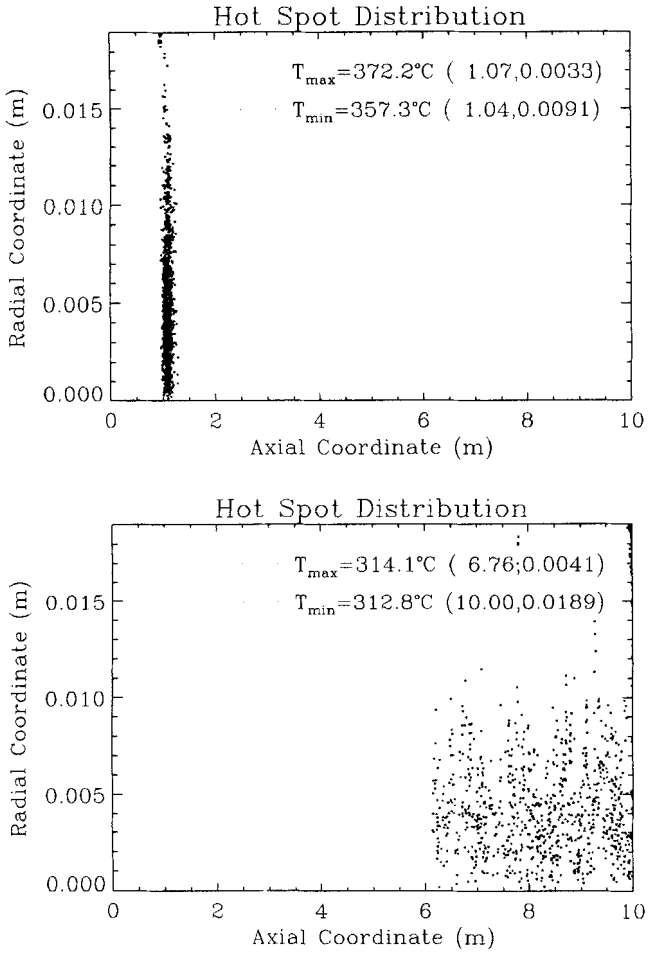

Figure 9. Hot-spot distribution in the tubular reactor with $C_\phi = 1.0$ (top) and $C_\phi = 1.5$ (bottom), and other parameters same as in Figure 8.

Each point marks the location where the hot spot occurred at each time step for the last 1,000 time steps of the simulation. The highest (T_{max}) and lowest (T_{min}) of these hot spots and their coordinates are given in the figure.

the simulation. In effect, this temperature represents a sample from the upper tail of the temperature pdf and could not be computed using traditional moment closures for the temperature field. In the figures, T_{max} and T_{min} are estimates of the upper and lower bounds of hot-spot temperature. These estimates are followed by the x and y coordinates of the actual locations of the extremal values in the tubular reactor.

As shown in Figure 9, $C_\phi = 1.0$ produces hot spots in the range of 357.3°C to 372.2°C compared to the mean final reaction temperature of only 307°C. Increasing C_ϕ to 1.5, the temperature range for hot spots is reduced to between 312.8°C and 314.1°C, which are approximately the same as the final mean temperature 313.7°C. Similar behavior is found with $C_\phi = 2.0$. It is also clear that the hot spots are strongly correlated with the high polydispersity values shown in Figure 8d. The highest polydispersity approximately coincides with the location of local hot spots. This information should be very useful in evaluating and improving reactor design. Since the standard value of C_ϕ is near unity, these simulations indicate the potential for reactor instability with center-mode injection. Increasing the flow rate (Reynolds number) would be one means of increasing the mixing rate. However, as discussed below, changing the injection mode may be equally as effective and entail lower operating costs.

Effect of initiator flow rate

The results for different initiator flow rates are shown in Figure 10. From Figure 10a it can be easily concluded that, since more initiator burns out instead of reacting with monomer before the reaction reaches steady state, the initiator efficiency decreases dramatically as the initiator flow rate increases. This is primarily due to the fact that increasing the initiator flow rate increases the reaction rate without changing the mixing rate. When the initiator flow rate relative to the monomer flow rate (F_I) is tripled from 0.0002 to 0.0006, the monomer conversion only increases from 4% to 5%. In fact, the simulations indicate that 5% is the highest value that can be achieved with these initial conditions (i.e., feed temperature, mixing rate, and injection mode). This suggests that in order to achieve higher monomer conversion, other parameters must be changed (such as lowering feed temperature, increasing mixing rate, or use uniform injection mode). Since initiator is a major cost item for LDPE production, such information should be very useful. However, increasing the initiator flow rate does improve the monomer conversion and shorten the length of the reaction zone as shown in Figure 10b and 10c. Furthermore, more initiator injection also leads to higher polydispersity as shown in Figure 10d, which should be considered carefully for polymer quality control. Although no hot spot was observed in these simulations, it should be noted that a higher initiator flow rate also increases the possibility of hot-spot formation. For example, the hot-spot distribution with $F_I = 0.0004$ shown in the top panel of Figure 9 disappeared when F_I was reduced to 0.0002.

Effect of inlet monomer temperature

It is well known that lowering the inlet temperature can increase monomer conversion and polymer quality dramati-

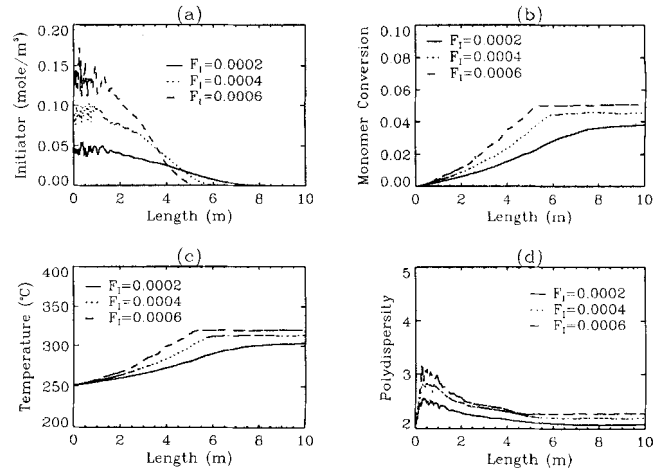

Figure 10. Radially averaged quantities vs. reactor length at different F_I with center-mode injection, $C_\phi = 2.0$, and $T_{inlet} = 252$°C.

The final values of λ_1 are 2,472 mol/m^3 (F_I = 0.0002), 1,940 mol/m^3 (F_I = 0.0004), and 1,598 mol/m^3 (F_I = 0.0006).

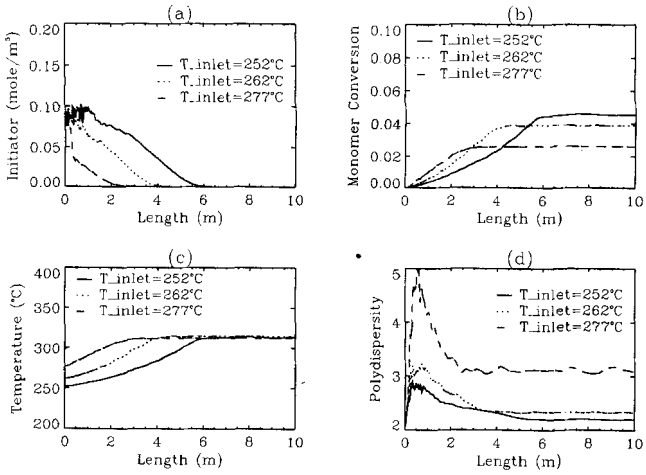

Figure 11. Radially averaged quantities vs. reactor length with different T_{inlet} with $C_\phi = 2.0$, center-mode injection, and $F_I = 0.0004$.

The final values of λ_1 are 1,940 mol/m^3 (T_{inlet} = 252°C), 1,736 mol/m^3 (T_{inlet} = 262°C), and 1,354 mol/m^3 (T_{inlet} = 277°C).

cally, but it also increases the reaction time and can extinguish the reaction completely. Figure 11 illustrates the effect of inlet temperature (T_{inlet}) on polymerization with center-mode injection, $F_I = 0.0004$, and $C_\phi = 2.0$. While the initiator is consumed gradually along the reactor with the inlet temperature at 252°C, it is mostly consumed at the beginning when the inlet temperature is 277°C. The higher initiator consumption results in a large decrease in monomer conversion as shown in Figure 11b. The effect on polydispersity is also dramatic as seen in Figure 11d. At the end of the simulation domain, the polydispersity for the highest inlet temperature is almost 50% higher than the value for the lowest inlet temperature. Since at higher temperatures the reaction rate for initiator decomposition (k_d) increases dramatically, the local micromixing rate is not sufficient to ensure that the monomer and initiator are well mixed.

Interestingly, the inlet temperature has little effect on the final mean reaction temperature. However, its effect on monomer conversion is much higher than that of micromixing or the initiator flow rate. Indeed, when the inlet temperature is decreased from 277°C to 252°C, the increase in the final mean reaction temperature is almost negligible, while the monomer conversion is almost doubled. The presence of hot spots near the reactor inlet at higher monomer feed temperatures (e.g., with T_{inlet} = 277°C, T_{max}, and T_{min} are 389°C and 381°C and located at $(x, y) = (0.36, 0.0012)$ m and (0.37, 0.0064) m, respectively), which are not found at lower inlet temperatures, leads to a lower initiator efficiency due to local burnout, and hence lower monomer conversion. As noted earlier, the presence of hot spots leads to a large increase in polydispersity, as is clearly seen in Figure 11d.

Effect of initiator injection mode

There is a great incentive due to the high cost of initiator to increase initiator efficiency. As can be seen from the simulation results presented thus far, this can be accomplished by avoiding hot-spot formation in the reactor. One way to do this is to increase the monomer flow rate in order to increase the Reynolds number and hence to increase the mixing rate (i.e., as Figure 8). However, increasing the flow rate will lead to increased capital and operating costs since a larger compressor would be required. Thus, there is significant economic incentive to find alternative solutions for avoiding initiator burnout. One simple design modification would be to improve the initiator injection nozzle. Since PDF methods are capable of full-field simulations, the effect of different initiator injection modes on hot-spot formation can be easily investigated. For our 2-D simulation domain, three injection modes have been investigated (see Figure 6): center-, ring-, and uniform-mode injection.

Simulations have been carried out to compare center-, ring-, and uniform-mode injection with $C_\phi = 2.0$, $F_I = 0.0004$, and $T_{inlet} = 277$°C. As shown in Figure 12, uniform- and ring-mode injection give almost identical results and produce higher initiator efficiency and smoother spatial gradients than center-mode injection. The polydispersity displays the most significant difference, as seen in Figure 12d. It is obvious that a more spatially uniform injection mode will result in better initiator efficiency and polymer quality without changing other operating parameters. Since the initiator flow rate is relatively small compared to the mean flow rate, the impact on the mean flow field when changing the injection mode should be minimal.

Theoretically, the plug-flow assumption (Eq. 18) represents the most ideal radial mixing condition available (albeit by ignoring axial dispersion) and should produce the highest monomer conversion. Shown in Figure 13 is the comparison between the plug-flow and uniform-mode injection results, with T_{inlet} = 252°C and the other conditions the same as in Figure 12. It is not surprising to find that the PDF simulation with uniform-mode injection results in a slightly lower monomer conversion. Since the plug-flow assumption neglects axial dispersion, the local PDF of reactive scalars, which contains the information about local mixing conditions, has zero variance. Therefore, the fluctuations in initiator concen-

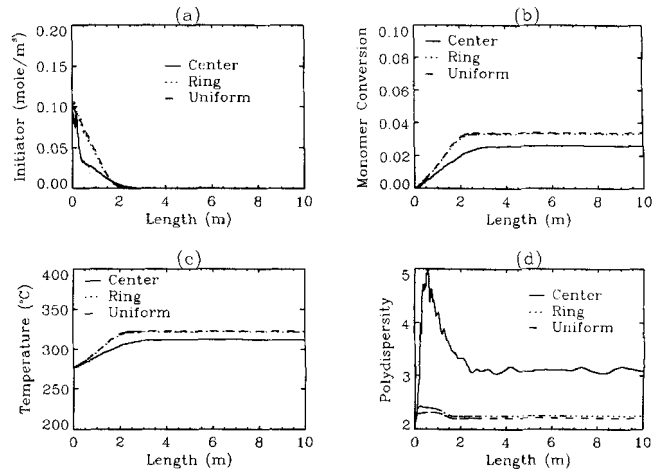

Figure 12. Radially averaged quantities vs. reactor length using different initiator injection modes with $C_\phi = 2.0$, $T_{inlet} = 277$°C, and $F_I = 0.0004$.

The final values of λ_1 are 1,354 mol/m^3 (center), 1,545 mol/m^3 (ring), and 1,565 mol/m^3 (uniform).

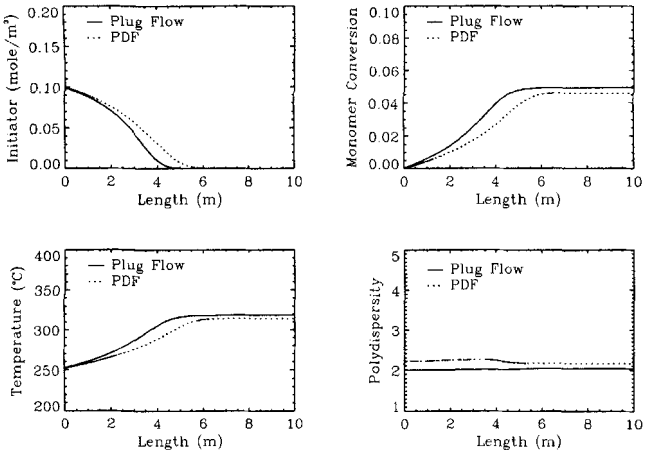

Figure 13. Axial profiles of initiator, monomer conversion, temperature, and polydispersity using the plug-flow model and the uniform-mode injection PDF simulation with $C_\phi = 2.0$, $T_{inlet} = 252°C$, and $F_I = 0.0004$.

The differences between the two curves are primarily due to the neglect of axial dispersion in the plug-flow model.

tration and polydispersity, which are caused by local poor mixing zones, cannot be predicted by plug-flow simulations. In general, it can be concluded that the plug-flow model is an adequate approximation if the initiator is distributed uniformly, but can result in significant errors otherwise (e.g., with center-mode injection).

In order to illustrate the effect of radial maldistribution near the injector, the initiator mean and rms fields for center- and ring-mode injection are shown in Figures 14 and 15 with $C_\phi = 2.0$, $T_{inlet} = 262°C$, and $F_I = 0.0004$. The surface plots show the magnitudes of initiator mean and rms. The radial gradients are visible in both figures. While center-mode injection produces very high radial gradients around the injection cell, ring-mode injection results in a faster radial spread of the initiator and also produces less fluctuations.

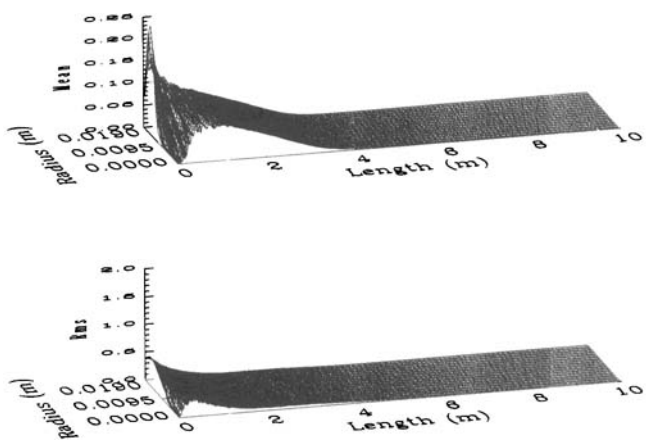

Figure 14. Initiator mean and rms fields with center-mode injection, $C_\phi = 2.0$, $F_I = 0.0004$, and $T_{inlet} = 262°C$.

The top and bottom surface plots are the initiator mean and rms fields, respectively.

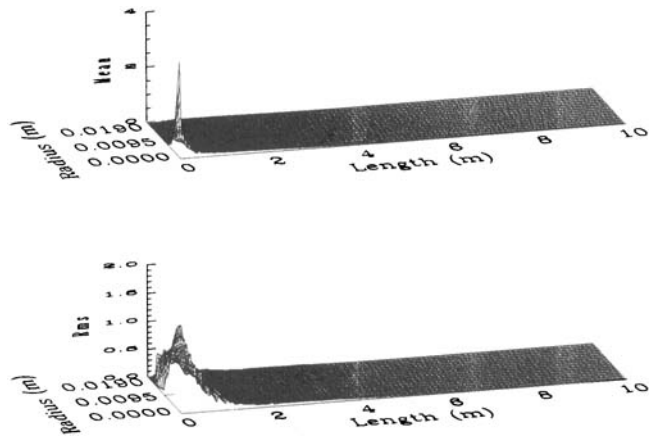

Figure 15. Same as in Figure 14, but with ring-mode injection.

Note the 16-fold difference in scale for the mean fields between this figure and Figure 14.

The competition between radial mixing and rapid initiator decomposition is won by the latter with center-mode injection resulting in a rapid burnout of the initiator. This fact is also reflected in the temperature fields: ring-mode injection not only produces a more uniform mean temperature field, but also results in a lower rms temperature. Due to its relationship to the spread of the temperature PDF, the lower rms temperature should decrease the possibility of forming local hot spots. These phenomena cannot be captured by models that ignore turbulent diffusivity (e.g., the plug-flow model), or concentration fluctuations (e.g., moment closures).

The hot-spot distributions reveal another important difference between injection modes: for the conditions in Figure 9, center-mode injection produces hot spots between 381.7°C and 389.3°C with a final mean reaction temperature of only 307°C, while the ring and uniform injection modes create virtually no local hot spots. Based on these results, one can conclude that radial gradients in the initiator field near the injection point should be avoided. Physically, this can be achieved by designing a "multi-point" injection nozzle that introduces initiator in the most radially homogeneous manner possible. Alternatively, a single nozzle with many radially (and slightly upstream) directed jets should yield satisfactory performance.

Conclusions

A first attempt at applying full PDF methods to simulate LDPE polymerization in a tubular reactor has been presented. Due to its ability to solve chemical-reaction terms without invoking moment closures, realistic free-radical polymerization kinetics can be combined with turbulence models to study the effects of turbulent mixing on LDPE polymerization. Unlike traditional phenomenological models and moment closure methods, full PDF methods are able to predict the effects of changing specific operating conditions, such as flow rate and initiator injection mode, which should be of great utility for the chemical process industry. Indeed, based on the simulations presented in this work, it was possible to make a specific design recommendation concerning the initiator injection nozzle. Given the highly competitive nature of

the LDPE market, such seemingly small improvements in reactor performance can lead to an important competitive advantage and hence increased profits.

Although detailed 3-D simulations are necessary to describe more complicated reactor geometries (viz., nonaxisymmetric), the 2-D simulations reported here are able to capture many important features of LDPE polymerization in tubular reactors. The combined PDF/CFD approach is readily applicable to more complicated geometries (viz., autoclave reactors). Using this technique, detailed time-resolved studies of the effect of different initiator injection locations and reactor designs on the polymerization process can be simulated. Although quantitative comparisons with experimental data are still difficult for LDPE reactors due to the difficulty of obtaining experimental data at such extreme operating conditions, the qualitative comparisons made in this study prove the feasibility of this new modeling technique. Furthermore, since the detailed flow field and spatial distribution of chemical reactants (including mean and rms fields, and extremal statistics) in a chemical reactor are obtained, this technique can provide valuable information for reactor design and modification for many other chemical processes.

The average CPU time for each simulation reported in this study was approximately 8 hours on a HP-APOLLO 735 workstation. Although still computationally intensive for 3-D simulations, it must be noted that Lagrangian PDF codes are naturally parallel. Thus, with the multiprocessor, parallel computer architectures now widely available, PDF computations of full 3-D geometries are readily feasible. More advanced PDF simulations of full 3-D chemical reactors with mechanical stirrers and heat exchange boundary conditions are currently under development and will be reported in future communications.

Acknowledgment

This work was supported by the National Science Foundation under grant CTS-9158124 (PYI Award) and The Dow Chemical Company.

Literature Cited

Bakker, A., and J. B. Fasano, "A Computational Study of the Flow Pattern in an Industrial Paper Pulp Chest with a Side Entering Impeller," *AIChE Symp. Ser.*, **89**, 118 (1993).

Bakker, A., N. Cathie, and R. Laroache, "Modeling of the Flow and Mixing in HEV Static Mixers," *Ind. Chem. Eng. Symp. Ser.*, **136**, 533 (1994).

Bilger, R. W., *Turbulent Reacting Flows*, Chap. 3, P. A. Libby and F. A. Williams, eds., Springer-Verlag, New York (1980).

Béquier, C., I. Dekerser, and B. E. Launder, "Ratio of Scalar and Velocity Dissipation Time Scales in Shear Flow Turbulence," *Phys. Fluids*, **21**, 307 (1978).

Chan, W. M., P. E. Gloor, and A. E. Hamielec, "A Kinetic Model for Olefin Polymerization in High-Pressure Autoclave Reactors," *AIChE J.*, **39**, 111 (1993).

Chen, J. Y., W. Kollman, and R. W. Dibble, "Pdf Modeling of Turbulent Nonpremixed Methane Jet Flames," *Combust. Sci. Technol*, **64**, 315 (1989).

Donati, G., L. Marini, G. Marziano, C. Mazzateri, M. Sampitano, and E. Langianni, "Mathematical Model of Low Density Polyethylene Tubular Reactor," *Proc. Int. Symp. Chem. React. Eng., Boston*, p. 579 (1982).

Dopazo, C., "Probability Density Function Approach for a Turbulent Axisymmetric Heated Jet Centerline Evolution," *Phys. Fluids*, **18**, 397 (1975).

Fox, R. O., "The Spectral Relaxation Model of the Scalar Dissipation Rate in Homogeneous Turbulence," *Phys. Fluids*, **7**, 1082 (1995).

Fox, R. O., "Computational Methods for Turbulent Reacting Flows in the Chemical Process Industry," *Rev. Inst. Fr. Pét.*, **51**, 215 (1996).

Gardiner, C. W., *Handbook of Stochastic Methods for Physics, Chemistry and the Natural Sciences*, Springer-Verlag, New York (1985).

Girimaji, S. S., "Assumed β-pdf Model for Turbulent Mixing: Validation and Extension to Multiple Scalar Mixing," *Combust. Sci. Technol.*, **78**, 177 (1991).

Goto, S., K. Yamamoto, S. Furui and M. Sugimoto, "Computer Model for Commercial High-Pressure Polyethylene Reactor Based on Elementary Reaction Rates Obtained Experimentally," *Appl. Poly. Symp.*, **36**, 21 (1981).

Heeb, T. G., and R. S. Brodkey, "Turbulent Mixing with Multiple Second-Order Chemical Reactions," *AIChE J.*, **36**, 1457 (1990).

Hrenya, C. M., E. J. Bolio, D. Chakrabarti, and J. L. Sinclair, "Comparison of Low Reynolds k-ϵ Turbulence Models in Predicting Fully Developed Pipe Flow," *Chem. Eng. Sci.*, **50**, 1923 (1995).

Jiang, T. L., and E. E. O'Brien, "Simulation of Scalar Mixing by Stationary Isotropic Turbulence," *Phys. Fluids A*, **3**, 1612 (1991).

Jones, W. P., and J. H. Whitelaw, "Calculation Methods for Reacting Turbulent Flows: A Review," *Combust. Flame*, **48**, 1 (1982).

Kiparissides, C., G. Verros, and J. F. MacGregor, "Mathematical Modeling, Optimization, and Quality Control of High-Pressure Ethylene Polymerization Reactors," *J.M.S.-Rev. Macromol. Chem. Phys.*, **C33**, 437 (1993).

Lapin, A., and A. Lübbert, "Dynamic Modeling of the Two-Phase Flow in Bubble Columns," *Proc. AIChE Meeting*, San Francisco (1994).

Laufer, J., "The Structure of Turbulence in Fully Developed Pipe Flow," *NACA Rep. 1174* (1954).

Launder, B. E., and D. B. Spalding, "The Numerical Computation of Turbulent Flows," *Comput. Methods Appl. Mech. Eng.*, **3**, 269 (1974).

Lee, K. H., and J. P. Marano, "Free-Radical Polymerization: Sensitivity of Conversion and Molecular Weights to Reactor Conditions," *ACS Symp. Ser.*, **104**, 221 (1979).

Leonard, A. D., R. M. Kerr, and J. C. Hill, "Evaluation of Closure Models for Turbulent Reacting Flows," *Ind. Eng. Chem. Res.*, **34**, 3640 (1995).

Marini, L., and C. Georgakis, "Low-Density Polyethylene Vessel Reactors," *AIChE J.*, **30**, 401 (1984).

Maas, U., and S. B. Pope, "Simplifying Chemical Kinetics: Intrinsic Low-Dimensional Manifolds in Composition Space," *Combust. Flame*, **88**, 239 (1992).

O'Brien, E. E., *Turbulent Reacting Flows*, Chap. 5, P. A. Libby and F. A. Williams, eds., Springer-Verlag, New York (1980).

Perng, C. Y., and J. Y. Murthy, "A Moving-Deforming-Mesh Technique for Simulation of Flow in Mixing Tanks," *AIChE Symp. Ser.*, **89**, 37 (1993).

Petzold, L. R., and A. C. Hindmarsh, "LSODAR: Livermore Solver for Ordinary Differential Equations, with Automatic Method Switching for Stiff and Nonstiff Problems, and with Root-Finding," Computing and Mathematics Res. Div., Lawrence Livermore National Lab., Livermore, CA (1987).

Pipino, M., and R. O. Fox, "Reactive Mixing in a Tubular Jet Reactor: A Comparison of pdf Simulations with Experimental Data," *Chem. Eng. Sci.*, **49**, 5229 (1994).

Pope, S. B., "A Monte-Carlo Method for the pdf Equations of Turbulent Reactive Flow," *Comb. Sci. Technol.*, **25**, 159 (1981).

Pope, S. B., "Pdf Methods for Turbulent Reactive Flows," *Prog. Energy Combust. Sci.*, **11**, 119 (1985).

Pope, S. B., "Lagrangian PDF Methods for Turbulent Flows," *Annu. Rev. Fluid Mech.*, **26**, 23 (1994).

Roekaerts, D., "Use of a Monte Carlo pdf Method in a Study of the Influence of Turbulent Fluctuations on Selectivity in a Jet-Stirred Reactor," *Appl. Scientif. Res.*, **48**, 271 (1991).

Rogers, M. M., N. N. Mansour, and W. C. Reynolds, "An Algebraic Model for the Turbulent Flux of a Passive Scalar," *J. Fluid Mech.*, **203**, 77 (1989).

Rubinstein, R., and J. M. Barton, "Nonlinear Reynolds Stress Model and the Renormalization Group," *Phys. Fluids A*, **2**, 1472 (1990).

Shirodkar, P. P., and G. O. Tsien, "A Mathematical Model for the Production of Low Density Polyethylene in a Tubular Reactor," *Chem. Eng. Sci.*, **41**, 1031 (1986).

Smit, L., "The Use of Micromixing Calculations in LDPE-Reactor Modeling," *DECHEMA Monogr.*, **127**, 77 (1992).
Tosun, G., "A Mathematical Model of Mixing and Polymerization in a Semibatch Stirred-Tank Reactor," *AIChE J.*, **38**, 425 (1992).
Tsai, K., and E. E. O'Brien, "A Hybrid One- and Two-Point Approach for Isothermal Reacting Flows in Homogeneous Turbulence," *Phys. Fluids A*, **5**, 2901 (1993).
Tsai, K., and R. O. Fox, "Pdf Simulation of a Turbulent Series-Parallel Reaction in an Axisymmetric Reactor," *Chem. Eng. Sci.*, **49**, 5141 (1994).
Tsai, K., and R. O. Fox, "PDF Modeling of Turbulent Mixing and Chemical Reactions in a Tubular Jet Reactor," *AIChE Symp. Ser.*, **305**, 31 (1995).
Tsai, K., and R. O. Fox, "Modeling the Scalar Dissipation Rate for a Turbulent Series-Parallel Reaction," *Chem. Eng. Sci.*, **51**, 1929 (1996).
van der Molen, Th. J., and C. van Heerden, "The Effect of Imperfect Mixing on the Initiator Productivity in the High Pressure Radical Polymerization of Ethylene," *Adv. Chem. Ser.*, **109**, 92 (1972).
Villermaux, J., and L. Blavier, "Free Radical Polymerization Engineering: I. A New Method for Modeling Free Radical Homogeneous Polymerization Reactions," *Chem. Eng. Sci.*, **19**, 87 (1984).
Yakhot, V., and S. A. Orzag, "Renormalization Group Analysis of Turbulence," *J. Sci. Comput.*, **1**, 3 (1986).
Yoon, B. J., and H. K. Rhee, "A Study of the High Pressure Polyethylene Tubular Reactor," *Chem. Eng. Commun.*, **24**, 253 (1985).
Zabisky, R. C. M., W. M. Chan, P. E. Gloor, and A. E. Hamielec, "A Kinetic Model for Olefin Polymerization in High-Pressure Tubular Reactors: a Review and Update," *Polymer*, **33**, 2243 (1992).

Manuscript received Feb. 5, 1996, and revision received Mar. 14, 1996.